SMAR 2019 – Fifth Conference on Smart Monitoring,
Assessment and Rehabilitation of Civil Structures

SMAR 2019

Comparison of cracks formed in scaled grouted connection of offshore energy structures under static and cyclic loads

Götz HÜSKEN [1], Md SHAMSUDDOHA [1], Marc THIELE [1], Matthias BAEßLER [1], Hans-Carsten KÜHNE [1]

[1] Bundesanstalt für Materialforschung und -prüfung (BAM), Berlin, Germany

Contact e-mail: goetz.huesken@bam.de

ABSTRACT: Global energy consumption will increase in the future necessitating both fossil fuels and renewable energy choices - especially wind energy. Such high energy demand requires installation of offshore energy structures, rigs, platforms and towers, which are susceptible to adverse environmental conditions along with maintenances. Due to their large size and remote locations, cylindrical grouted joints are often adopted between substructure and foundation in these offshore platforms and wind structures such as monopiles. However, these connections are composite structures with exterior sleeve, interior pile and infill mortar. Degradation and settlements were reported inside similar connections, which were installed in last three decades. Besides, grouting in the offshore sites were proven difficult to obtain ideal load bearing capacity. In-situ loading conditions were also found to be affecting the failure mechanism inside such connections. This study aims at characterizing the nature of cracks generated in these grouted connections under both static and cyclic loading. Scaled grouted joints were manufactured using a novel reusable mold, and connections were loaded to failure to visualize the main failure patterns. An assessment between failure under these two types of load is drawn along with comparison to previously available literature.

1 INTRODUTION

The World Energy Outlook estimates a growth of about 30% in the worldwide energy demand by the year 2040 (International Energy Agency 2014). Although, oil and gas (O&G) sector may well dominate the global primary energy supply for the rest of this century, energy security issues are directing countries towards renewable energy choices, which can reduce their dependency on fossil fuels as well as achieving sustainable energy future (Larsen et al. 2010). Hence, a future of sustainable energy demands substitution of fossil fuels by renewable energy sources around the world. The contribution of renewable energy sources in primary energy use, suggested by the New Policies Scenario, is raised to 18% in 2035 compared to 13% in 2011, where wind energy is expected to provide major share, limiting the rapid growth of traditional fossil fuels (International Energy Agency 2013). Therefore, growing energy demand and advancement of technology lead to explore both onshore and offshore locations using wind structures, which are susceptible to adverse loading conditions and costly maintenance.

There are three common types of piles that are used for fixed offshore wind turbine generators (WTG) structures, namely: i) Main and Skirt piles, ii) Cluster piles and iii) Monopiles. Monopile structures are currently the most preferred option for WTG structures. These tubular towers occupy the wind turbine market due to their suitability in terms of economy, aesthetic and safety. The connections between the superstructure and the substructure can be either ring

welded and bolted in the flanges. However, fabrication of flanges is very costly and takes a long delivery time along with the disadvantages of fatigue damage over time (Verma 2011). Besides, the transition between the monopile and upper structure poses challenges, which can be addressed using infilled sleeved connections. As a result, grouted connections are often sought for the wind and offshore energy structures all over the world. Figure 1 shows a typical grouted connection between the upper structure and the monopile foundation. These connections are formed by filling the annulus with grout between the two members with dissimilar dimensions, where the infill acts as a load transfer medium. These grouted joints have been effectively used in the offshore drilling and production platform jackets and wind turbine structures.

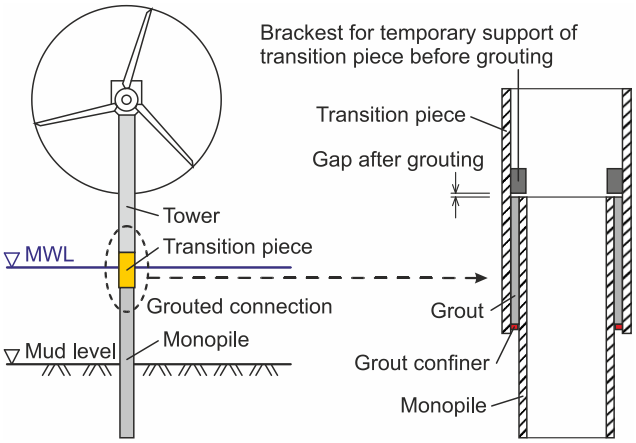

Figure 1. A typical grouted connection in monopile tower according to Lotsberg (2013).

In general, the grouted connections are susceptible to degradation due to repetitive adverse bending moments in conjunction with axial loading including fabrication challenges (Faulkner 2013; Hassanzadeh 2012). In last three decades, grouted joints have been installed in offshore wind energy structures, especially monopiles, using plain steel sections with no additional mechanical interlock. However, vertical displacements have been noticed at these connections. Schaumann et al. (2010) indicated that this movement might be resulting from a loss of bond between steel and mortar suggesting a repair option by applying several bearing mechanisms. In another study later, Schaumann et al. (2013) concluded that higher flexibility in response to bending loads lead to gap openings and relative sliding motion between adjacent material surfaces causing abrasive wear of the grout, which can considerably reduce the service life. Besides, increase in wear rate for various conditions including presence of water at an order of 2 - 18 times higher than for the equivalent dry condition, which may reduce the coefficient of friction below the value recommended by Dallyn et al. (2016). Hence, potential repair options should be sought after for any degradation in these structures especially the infill itself. To achieve this goal, it is necessary to characterize the failure patterns for selection of any repair option. The aim of this study is to conduct a feasibility study of producing failure patterns similar to degraded structures under axial load. This study is a preliminary stage of actualizing the failure pattern of such grouted connection using a novel reusable mold connection.

2 CONNECTION GEOMETRY, MATERIALS AND TEST DETAILS

2.1 Scaled Grouted Connection

In all jointing methods, the transition piece from the superstructure encircles the foundation pile or vice versa. Generally, there are two types of grouted connection systems in terms of load

transfer mechanism - 'plain' connection and 'with shear keys' connection that are intensively applied in the industry. The plain grouted joint is the earliest form of connection for joining foundation and superstructure. However, the geometry of the joint can be either tubular or conical in shape depending on the suitability in various structures (Wilke 2014). Mechanical connectors, such as shear keys in the form of welded beads or bars, can be introduced to increase bond strength of these joints. Shear keys are advantageous over plain connections (Ingebrigtsen et al. 1990). There can be different combinations of geometries and shear key provisions applicable to the tubular connections. However, according to DNV-OS-J101 (DNV 2014) and DNVGL-ST-0126 (DNV 2016), a grouted joint in wind energy monopile should not combine conical shape with shear keys. This standard also provides design guidelines of grouted joints in monopile structures based on different geometries and shear key provisions. In this study, a cylindrical connection with shear key was selected. A scaled grouted connection, which can be used in the laboratory for producing control cracks, was manufactured.

The sizes of the members vary depending on type of structures, purpose and locations. A detailed range of geometries used by previous researchers is given by Dallyn et al. (2015a). Due to simplicity of testing, a scaled test setup was used. Besides, the loading for this preliminary test was planned to be below 1 MN. However, it is to be noted that a more realistic grout layer was adopted, since one of the aims was to observe the crack pattern in the infill layer. This also implies that size of the pile and sleeve would be scaled down slightly disproportionately. For this study, a joint geometry was chosen after Chivato et al. (2014) as a reference.

Details of the mold geometry are given in Figure 2. The pile is one piece cylindrical core. The sleeve is built up from two equal parts and externally clamped with five external couplings with bolts. The couplings of the specimen are 30 mm wide, 30 mm thick and have a 180 mm thick flange. Clamps were bolted with Class 8.8 M18 bolts, whose minimum tensile strength is 800 MPa.

Table 1. Symbols and scaling factors of the scaled grouted connection

Definition	Symbol	Actual (mm)	Adopted (mm)	Scale
Sleeve outer diameter	D_s	1800	216	8.33
Wall thickness of sleeve	T_s	60	16	3.75
Pile outer diameter	D_p	1050	70	12.73
Wall thickness of pile	T_p	50	16	3.13
Grout outer diameter	D_g	1680	184	9.13
Thickness of grout	T_g	315	50.75	6.21
Shear key outstand	h	12	2.5	4.80
Shear key spacing	S	300	50	6.00
Shear key width	w	20	5	4.00

The sleeve was split into half for two reasons: firstly, for ease of creating shear keys inside sleeve interior with precise dimensions, and secondly, to make the mold reusable since the sleeve would not have to be cut to see internal cracks similarly to previous studies. The length of the joint is chosen such that three shear key pairs are accommodated to observe the failure criteria. The comparison of the selected size and the actual size is shown in Table 1. For ease of understanding, connection components are named as Pile (p), Grout (g) and Sleeve (s). The symbols used for geometric dimensions are similar to that of DNV-OS-J101 (DNV 2014) and DNVGL-ST-0126 (DNV 2016). The reason for such scaling is that, after scaling down of the members, grout layer will still remain closely representative of full-scale grout thickness similar

to that adopted earlier by Dallyn et al. (2015b). The guidelines by current DNVGL-ST-0126 (DNV 2016) for geometric parameters were adhered to where possible. Nevertheless, the size (radius) of the shear key is kept 2.5 mm, which is less than DNV practice. However, it was done so to be proportional to other reduced dimensions of components of the connection.

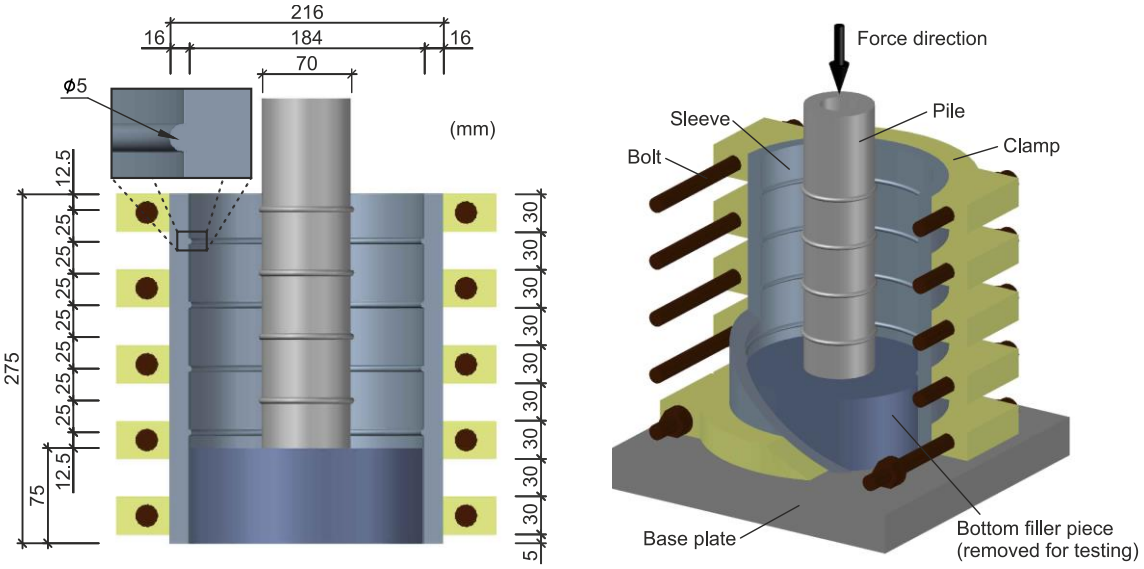

Figure 2. Schematic of the test mold.

The mold was manufactured using steel with a yield strength of 355 MPa. A commercial grout was applied as infill. The workability of the fresh grout was tested directly after mixing according to DIN EN 1015-3:2007 using the Hägermann cone. Specimens were removed from molds after one day and cured underwater at 23 °C before determining hardened grout properties after 28 days. It is to be noted that 40×40×160 mm prismatic specimens were used conforming European Standard DIN EN 196-1:2016 to determine compressive strength, whereas current DNV-OS-J101 (DNV 2014) practice suggests for 75 mm cube specimen. The reason for choosing prismatic samples is caused by the fact that prism strength was found closely aligned with cube specimens earlier (Schaumann et al. 2016). Furthermore, Young's modulus and drying shrinkage was determined according to DIN EN 12390-13:2014 and DIN EN 12617-4:2002, respectively. A summary of the properties of the fresh and hardened grout is given in Table 2.

Table 2. Characteristics of the infill grout in fresh and hardened state.

Property	Standard DIN	Infill Grout
Workability (mm)	1015-3	305
Compressive strength (MPa)	196-1	112 - 116
Flexural strength (MPa)	196-1	12 - 13
Young's modulus (MPa)	12390-13	40
Drying shrinkage at 28 days (%)	12617-4	0.07

2.2 Test Setup

No sand blasting or surface treatment was applied to the specimen. The test specimen was filled up with grout and kept at 23 °C with a relative humidity of 50% for 28 days prior to testing. The grouted connections were tested about 28 days after casting using a 1 MN MTS servo-hydraulic testing machine (see Figure 3). Static axial loading was applied at a rate of 0.15 mm/min. The loading was continued until cracks were generated or a plateau in loading response was observed. The loading program suggested by Thiele et al. (2016) was applied for cyclic loading. This program consists of a sine function with a frequency of about 5 Hz and is further defined by the minimum (S_{min}) and maximum (S_{max}) load as well as the mean (S_m) load. The corresponding values, considering a failure load (F_{max}) of about 820 kN as determined by the static tests, amount to $0.2\times F_{max}$, $0.65\times F_{max}$ and $0.425\times F_{max}$ for the first level of cyclic loading (about 1.9×10^6 cycles) and were increased to $0.225\times F_{max}$, $0.675\times F_{max}$ and $0.45\times F_{max}$ for the second level until a total displacement of 3 mm was obtained after further 1.9×10^6 cycles.

The sine function was interrupted every 7000 cycles for measuring the total vertical deformation of the grouted connection. For this purpose, different force-controlled loading ramps were applied including a complete loading and unloading of the specimen. Data acquisition was carried out using 3 Linear Displacement Transducers (LVDTs). The mean displacement was calculated from the 3 LVDTs and is used for the corresponding load-displacement plots. A summary of the specimens and the corresponding test parameter is given in Table 3.

Table 3. Summary of specimens and test parameters.

Specimen	Test parameter
Static 1	Static loading with 1.4 mm total displacement
Static 2	Static loading with 1.6 mm total displacement
Static 3	1st test: static loading up to 800 kN 2nd test: static loading (reloading) with 3.3 mm total displacement
Static 4	Static loading with 3.3 mm total displacement
Cyclic 1	Cyclic loading

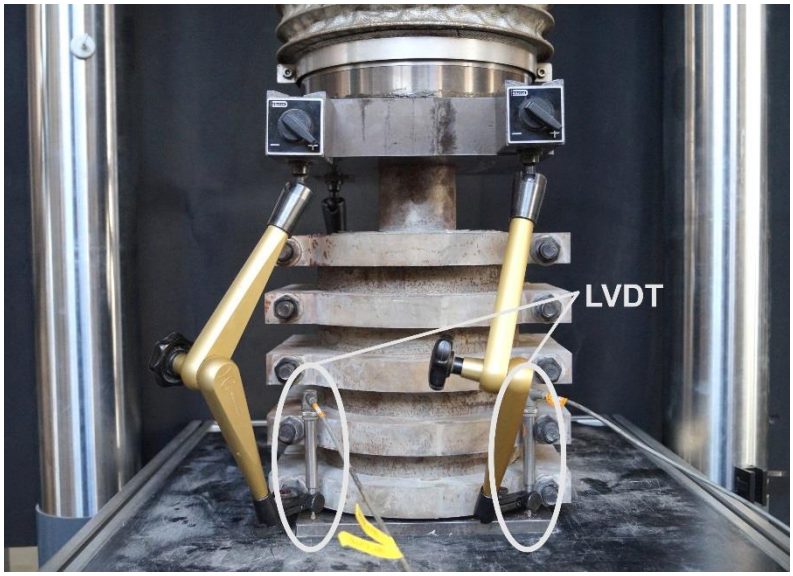

Figure 3. Specimen placed in the servo-hydraulic testing machine.

3 RESULTS AND DISCUSSION

3.1 Load Response under Static Load

Figure 4 shows the load-displacement plots of the specimens under uniaxial static load. The loading response can be divided into four primary segments. Firstly, the initial instrumental adjustment under loading occurred until about 0.2 mm, beyond which the loading response is straight in nature up to about 500 - 825 kN at a displacement of about 0.3 - 0.8 mm. Further loading generated relatively higher deformations and the load-displacement plot is no longer straight with a peak load at about 0.6 - 1.0 mm. Specimen 1 and 2 have peak loads of about 824 kN and 910 kN, respectively. To draw a comparison, according to DNV-OS-J101 (DNV 2014), the shear capacity considering a monopile structure without factor of safety is about 930 kN. This load calculation assumes that the sleeve is homogeneous without any split. It should be noted that there can be deviation between these experimental results and DNV guideline due to the variation in stiffness for adopting external couplings for split sleeves. The load-displacement is relatively straight before leading to a peak load. Finally, beyond peak, the curves drop gradually to 0.84 - 0.91×F_{max} and increase slightly again for larger deformations.

Specimen 3 was loaded twice to study the reloading behavior. Therefore, the specimen was firstly loaded up to 800 kN, below which the loading pattern was found elastic for previous specimens, and fully loaded again after complete unloading. The load bearing behavior of the first loading corresponds well to the linear behavior of the other specimens and the deviation among the specimens is small in this phase. However, the reloading of the specimens shows that the stiffness of the grouted connection increases and the total deformation decrease at comparable loading.

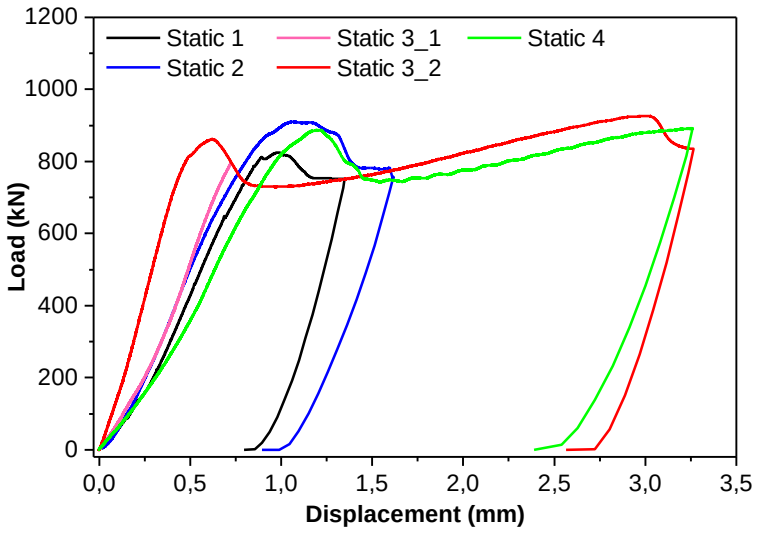

Figure 4. Load-displacement behavior under static loading.

3.2 Load Response under Cyclic Load

Figure 5a shows the load-displacement plot of specimen ‘Cyclic 1’. The grouted connection shows different behavior for both levels. At Level 1, the total displacement increases within few cycles in the beginning and reaches a constant value with just a minor increase of the total displacement. At the beginning of Level 2, the limits of the cyclic loading were increased,

which also increased the total displacement of the first load cycle. In contrast to Level 1, the total displacement at Level 2 increases over the entire period of cyclic loading with remarkable increase that occurs during the first few cycles of Level 2. Similar deformation behavior under cyclic loading was reported by Anders (2007). The calculated stiffness depicted in Figure 5b represents the resulting force at S_{min} divided by the corresponding deformation determined at the force-controlled loading ramps used for measuring purpose. The development of the stiffness over the applied loading cycles is strongly coupled with the deformation behavior. Here, increasing deformations result in decreasing stiffness, while an increase in the stiffness of the grouted connection reduced the corresponding deformation. Most likely, the increase in the stiffness is mainly be caused by the compressed concrete near the upper shear keys.

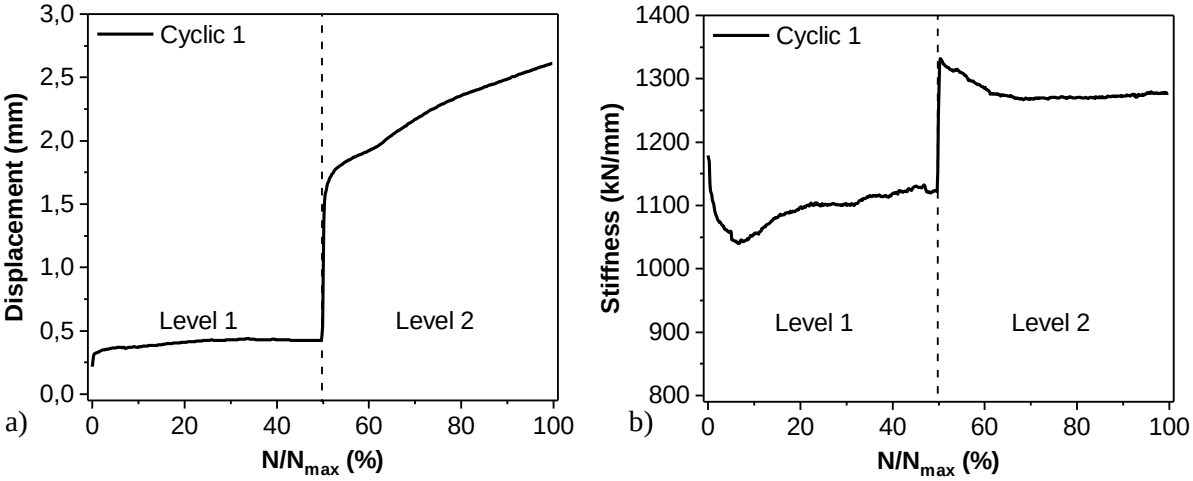

Figure 5. Behavior under cyclic loading: a) Total displacement; b) Calculated stiffness.

3.3 Failure Pattern

The internal cracks for specimen 'Static 1' are shown in Figure 6a. Two larger cracks are distinctly visible in the lower part of the specimen. The bottom crack is extended from the lowest shear key of the sleeve and the pile. However, the longer second crack on top is extended between the lowest key of the sleeve to the immediate upper shear key. There was no significant slippage near shear keys probably due to the high strength grout used. This is evident from the compressed grout with dark appearance below the top shear keys. This failure pattern and condensing in grout phenomenon are exactly similar to the cracks observed by Anders (2007). These cracks are, however, not perfectly extended between successive diagonal keys as seen in earlier studies (Billington & Lewis 1978, Sele et al. 1989). The reason, again, can be due to the use of low strength grouts in these past studies.

The crack pattern of the specimen under cyclic load is shown in Figure 6b. The cyclic load caused more aggressive cracks between the shear keys. The crack patter under cyclic load is characterized by cracking along struts of the lower shear keys and grout matrix failure in terms of compressed grout near the upper shear key. The crack pattern of the own tests under cyclic load is in line with the observations reported by Anders (2007).

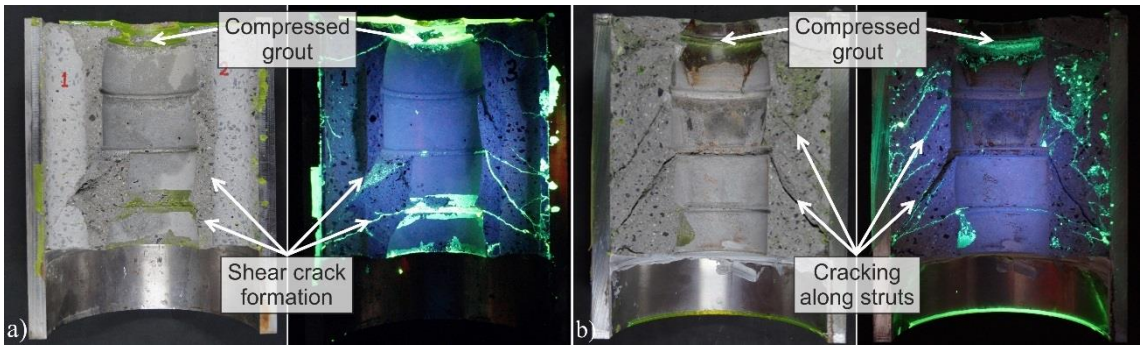

Figure 6. Internal failure pattern: a) static loading (Static 1); b) cyclic loading (Cyclic 1).

4 CONCLUSIONS

A reusable novel grouted connection mold with steel sleeve and pile, and grouted infill was manufactured and tested under uniaxial static and cyclic loads to study the feasibility of producing failure pattern. The load-bearing behavior and failure patterns were observed. The load-bearing capacity of the connection under static loading was found to be about 90% of the calculated shear capacity suggesting the fact that similar connection can be used for future experimental investigation. The failure pattern determined both for uniaxial static and cyclic loading was representative of results reported previously in the literature. However, the test specimens are scaled down from actual dimensions. Hence, there may be deviation in failure pattern with large full-scale structures. Besides, further investigation is needed for failure pattern and repair performance in connections under cyclic loads in the future. This implies also testing grouted connections in submerged condition.

ACKNOWLEDGMENTS

This study was undertaken under the LeBeWind project carried out in Federal Institute for Materials Research and Testing (BAM) and funded by the Federal Ministry for Economic Affairs and Energy (BMWi), Germany.

REFERENCES

Anders, S. 2007. Betontechnologische Einflüsse auf das Tragverhalten von Grouted Joints, PhD thesis, Gottfried Wilhelm Leibniz Universität Hannover, Germany.

Billington, C.J. and Lewis, G.H. 1978. The Strength of Large Diameter Grouted Connections, in 'Offshore Technology Conference', The Society of Petroleum Engineers, 8-11 May, Houston, Texas.

Chivato, R., Kougioumtzoglou, M. and Sanchez, N. 2014. Industrial Case Study: Finite Element Model, Jacket Substructures for Offshore Wind Turbines and Pre-piled Grouted Connections, University of Strathclyde, Glasgow'. website visited 17.01.2018. http://www.esru.strath.ac.uk/EandE/Web_sites/13-14/Jacket Substructures/grouted/modfinitelement.html

Dallyn, P., El-Hamalawi, A., Palmeri, A. and Knight, R. 2016. Experimental investigation on the development of wear in grouted connections for offshore wind turbine generators, *Engineering Structures*, 113, 89–102.

Dallyn, P., El-Hamalawi, A., Palmeri, A. and Knight, R. 2015a. Experimental testing of grouted connections for offshore substructures: A critical review, *Structures* 3, 90–108.

Dallyn, P., El-Hamalawi, A., Palmeri, A. and Knight, B. 2015b. Development of a Numerical Model to Predict Wear in Grouted Connections for Offshore Wind Turbine Generators, *International Journal of Civil and Environmental Engineering* 9(2), 122–131.

DNV (2014). Design of Offshore Wind Turbine Structures - DNV-OSJ101, Standard. Det Norske Veritas (DNV).

DNV (2016). Support structures for wind turbines - DNVGL-ST-0126, Standard. DNV GL AS.

Faulkner, P. and Hassel, M. 2013. Structural health monitoring systems on offshore wind turbine structures, in 'European Wind Energy Conference and Exhibition – EWEC 2013', Vol. 2, Elsevier B.V., 4-7 February, Vienna, Austria, Vienna, Austria, 1175–1181.

Hassanzadeh, M. 2012. Cracks in onshore wind power foundations: Causes and consequences, Elforsk rapport 11-56, Technical report, Elforsk AB, 101 53 Stockholm, Sweden.

International Energy Agency. 2014. World Energy Outlook, Technical report, IEA, 9 rue de la Fédération, 75739 Paris Cedex 15, France.

International Energy Agency. 2013. World Energy Outlook, Technical report, IEA, 9 rue de la Fédération, 75739 Paris Cedex 15, France.

Larsen, H. and Petersen, L.S. 2010. Non-fossil energy technologies in 2050 and beyond, Risø National Laboratory for Sustainable Energy, Technical University of Denmark, Denmark.

Lotsberg, I. 2013. Structural mechanics for design of grouted connections in monopile wind turbine structures, *Marine Structures*, 32, 113-135.

Schaumann, P., Lochte-Holtgreven, S., Lohaus, L. and Lindschulte, N. 2010. Durchrutschende Grout-Verbindungen in OWEA - Tragverhalten, Instandsetzung und Optimierung, *Stahlbau,* 79(9), 637–647.

Schaumann, P., Lochte-Holtgreven, S., Eichstädt, R., Camp, T. and Mc-Cann, G. 2013. Numerical Investigations on Local Degradation and Vertical Misalignments of Grouted Joints in Monopile Foundations, in 'The Twenty-third International Offshore and Polar Engineering Conference', International Society of Offshore and Polar Engineers, 30 June - 5 July, Anchorage, Alaska, 164–179.

Sele, A., Veritec, A. and Kjeóy, H. 1989. Background for the New Design Equations for Grouted Connections in the DNV Draft Rules for Fixed Offshore Structures, in 'Offshore Technology Conference', The Society of Petroleum Engineers, 1-4 May, Houston, Texas.

Thiele, M., Petryna, Y. and Rogge, A. 2016. Experimental investigation of damage evolution in concrete under high-cycle fatigue, 9th International Conference on Fracture Mechanics of Concrete and Concrete Structures – FraMCos-9, 29 May - 1 June, Berkeley, California, USA

Verma, A. 2011. Adhesive Bonded Towers for Wind Turbines - Design, Optimization and Cost Analysis, Master's thesis, Delft University of Technology, Delft, The Netherlands.

Wilke, F. 2014. Load Bearing Behaviour of Grouted Joints Subjected to Predominant Bending, PhD thesis, Gottfried Wilhelm Leibniz Universität Hannover, Germany.